Morphologies Observed in Ultraflexible Microemulsions with and without the Presence of a Strong Acid

Tobias Lopian, Sebastian Schoettl, Sylvain Prevost, S Pellet-Rostaing, Dominik Horinek, Werner Kunz, Thomas Zemb

ACS central science

Research Article

http://pubs.acs.org/journal/acscii

Morphologies Observed in Ultraflexible Microemulsions with and without the Presence of a Strong Acid

Tobias Lopian,[†,‡] Sebastian Schöttl,[‡] Sylvain Prévost,[§] Stéphane Pellet-Rostaing,[†] Dominik Horinek,*[,‡] Werner Kunz,[‡] and Thomas Zemb[†]

[†]Institut de Chimie Séparative de Marcoule, UMR 5257(CEA/CNRS/UM2/ENCSM), 30207 Bagnols sur Cèze, France

[‡]Institute of Physical and Theoretical Chemistry, University of Regensburg, 93040 Regensburg, Germany

[§]ESRF—the European Synchrotron Radiation Facility, 38000 Grenoble, France

Supporting Information

ABSTRACT: We show that three different morphologies exist near the two-phase boundary of ternary systems containing a hydrotropic cosolvent. Based on synchrotron small- and wide-angle X-ray scattering combined with molecular dynamics, we rationalize the specific scattering signature of direct, bicontinuous, and reverse mesoscale solubilization. Surprisingly, these mesostructures are resilient toward strong acids, which are required in industrial applications. However, on a macroscopic scale, the phase boundary shifts in salting-in and salting-out in the direct and respectively reverse regime, leading to a crossing of the binodals.

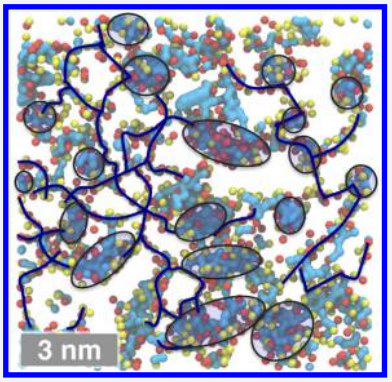

INTRODUCTION

Water and octan-1-ol (for simplicity referred to as octanol) are essentially nonmiscible, but upon addition of ethanol, the miscibility gap can be closed. The formation of organized aggregates was observed in the monophasic region of the phase diagram close to the phase boundary using light scattering techniques, and was referred to as the pre-Ouzo effect,[1] which has also been described as "mesoscale solubilization".[2] To ensure that this is not simply a critical effect, this phenomenon was further investigated by small-angle X-ray and neutron scattering experiments.[3] Variation of the contrast allowed detecting an accumulation of ethanol at the interface. These results have been confirmed by molecular dynamics simulations, which demonstrated that ethanol is present in both phases and is enriched at the interface.[4] Moreover, it was possible to show that the pre-Ouzo aggregates have preferable sizes, which is untypical for critical effects. Thus, the presence of well-defined, swollen micelle-like aggregates with weak intermolecular interactions has been proven. They are composed of mainly octanol, ethanol, and, to a lesser extent, water.

The pre-Ouzo effect is a quite general phenomenon that was also observed in alternative aqueous systems with fragrances,[5] insect repellents,[6] or green organic solvents[7] as organic counterparts. Thus, a generalization for the occurrence of the effect has been formulated: the pre-Ouzo phenomenon is observed in systems containing two solvents, "A" and "B", that are mutually not miscible and a third one, "C", that is miscible with both.[8] The term *detergentless* microemulsions has been introduced as concluded from their large solubilization power, which makes them even suitable as media for enzymatic reactions,[9] and from moderate resistance toward ultracentrifugation, leading to a Winsor-III type of phase separation.[10] Recently, the term *ultraflexible microemulsions* has been coined and a theoretical framework based on a balance of entropy and hydration forces has been developed.[8,11]

Since the interfacial film is enriched by hydrotrope molecules, any ion present at the interface can be a "perturbing" ion, but also ions in the aqueous pseudophases, as explained with a general concept introduced recently.[12] Combined X-ray, neutron, and light scattering studies have shown that the microstructuring can transform gradually into aggregates resembling "ordinary" microemulsions, by adding so-called antagonistic salts.[13]

The formation of mesoscopic structures in neat and wet octanol, the most studied solvent for ultraflexible microemulsions (UFME) so far, has been a long-time discussion when it comes to understanding the success and efficiency of the log(K_p) model:[14] the partition of a solute between water and 1-octanol, to determine its affinity toward organic or aqueous phases. In this context it has been revealed by direct (X-ray scattering/diffraction[15]) and indirect[16−18] structure analysis methods that spherical reverse aggregates with tail-to-tail arrangement of octanol molecules are present in wet 1-octanol. With the help of molecular dynamics,[19−21] it was

Received: April 19, 2016
Published: July 11, 2016

DOI: 10.1021/acscentsci.6b00116
ACS Cent. Sci. 2016, 2, 467−475

shown that the actual mesoscopic inhomogeneities in wet octanol are more complicated, since there are many different shapes and sizes of aggregates present. However, Chen and Siepmann demonstrated that spherical aggregates with aggregation numbers from 4 to 6 dominate the statistical distribution in wet 1-octanol, which thus confirms the outcome of the experimental results.[21]

Based on conductivity measurements, it was postulated that not only one but possibly *four* different types of regions are present in the monophasic domain of the ternary phase system 1-octanol/ethanol/water at different compositions.[22] In the two phase domain of the phase triangle, we use the term *phase* for compositions at the edge of the equilibrium state. If spontaneous emulsification takes place, we refer to compositions after slight centrifugation (at approximately 1000 rpm). In a macroscopically homogeneous single phase domain, we consider the aggregates and the external medium as pseudophases, as was done for the case of micelles and bilayers by Charles Tanford[23] and quantitatively developed by Israelachvili, Mitchell, and Ninham for classical surfactants.[24] In this picture, the nonhomogeneous distribution of ethanol in the core or close to the w/o interface is simply averaged.[25] Besides a molecular solution and the direct pre-Ouzo clusters, the possible presence of bicontinuous and reverse structures was reported. However, electrical conductivity data only allows a macroscopic interpretation of results, and a hypothesis on structuring on a molecular scale was thus ambiguous. It is worth noting that, to our knowledge, the region on the octanol-rich side of the phase diagram has not been studied yet by X-ray, so no structural reference was known before the present study.

For the first part of this work, two fundamental questions were raised: First, does the structuring of 1-octanol/water mixtures remain present when a component, here ethanol, which closes the miscibility gap between water and octanol, is added? The second question raised was: In case of a stable structuring in the presence of a hydrotrope, is there a transition of the continuous phase via bicontinuous structures in the gap between the direct pre-Ouzo regime and the reverse regime?

We use as model system octan-1-ol/ethanol/water mixtures, since thermodynamic data as well as the solubility of many added solutes are available.[26−28] We want to extend the previous analysis to regions all around the phase transition border, using a comparative experimental and theoretical approach. To do this, small and wide-angle X-ray scattering experiments (SWAXS) have been performed to reveal the structuring of the yet uninvestigated part of the phase diagram. To avoid ambiguity on the interpretation of the spectra, complementary molecular dynamics simulations (MD) have been performed.

Morphological transitions of weak aggregates induce the emergence of new properties in complex fluids. For instance, weak aggregates of extractants can be ordered or less ordered,[29] where weak aggregation is defined as any morphological transformation that is linked to less than 1 k_BT per molecule.[30] Moreover, it has been shown very recently that mesoscale ordering of weak aggregates originates from attractive interactions already on a molecular level.[31] In this work, a comparative analysis of MD simulations, theoretical predictions from electrostatic theory, and experimental SWAXS have been brought together to explain the correlation of attractive interactions between supramolecular structures and the molecular organization of the weak aggregate.

From a more practical point of view, phase separation and the structuring in the phases is crucial for extraction and recycling processes of metals as salts or nonelectrolytes. Therefore, in the second part of this work, we investigate how UFME are modified in their microstructure and properties in the presence of a further additive: sulfuric acid. This acid not only is of industrial interest but also is an example of a system containing a divalent ion, for which colloidal long-range interactions beyond the first neighbors[32] have been identified.[33] In this context, we focus on the following questions in the second part of this work: How is the miscibility gap modified in the presence of sulfuric acid, and what are the weak molecular interactions behind the variation of the liquid−liquid phase separation observed? Further: How does the addition of an electrolyte influence the microstructuring near the phase boundary? To answer these questions, the pseudoternary phase diagrams have been determined with varying amounts of added sulfuric acid, and SWAXS with and without sulfuric acid has been performed.

RESULTS AND DISCUSSION

Reverse Aggregation on the Octanol-Rich Part of the Phase Diagram. The primary subject of our study was the analysis of the mesoscopic structuring around the binodal for the ternary system 1-octanol/ethanol/water. X-ray scattering techniques are among the few suited methods for probing structure transitions in surfactant-free microemulsions. SWAXS is particularly appropriate, as it yields information from the atomic scale (high Q-values) up to the nano- and mesoscopic scale (low Q-values).

In Figure 1, five different experimental SWAXS spectra are shown for 1-octanol with and without the presence of water

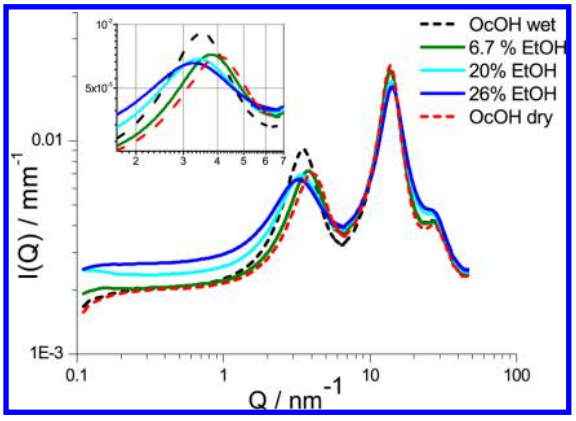

Figure 1. SWAXS spectra of "dry" 1-octanol (red dashed line), wet 1-octanol (5 wt % water, black dashed line), ternary system sample 1 (2.9 wt % water, 6.7 wt % ethanol, green curve), ternary system sample 2 (8.6 wt % water, 20 wt % ethanol, cyan curve), and ternary system sample 3 (11.4 wt % water, 26.7 wt % ethanol, blue curve). The compositions of the samples are also represented in Figure 2i as crosses.

and/or ethanol. In the WAXS regime, above 7 nm^{-1}, the curves converge and two peaks are visible. These correspond to the aliphatic and aqueous structure factors of molecular packing, with an intense signal to be found at 14.7 nm^{-1} and a less pronounced peak at 28 nm^{-1}.

In the small-angle regime below 7 nm^{-1}, all spectra show a characteristic peak, around ∼3.5 nm^{-1} (focused inside the small box of Figure 1), which, according to Franks et al., is a pair

DOI: 10.1021/acscentsci.6b00116
ACS Cent. Sci. 2016, 2, 467−475

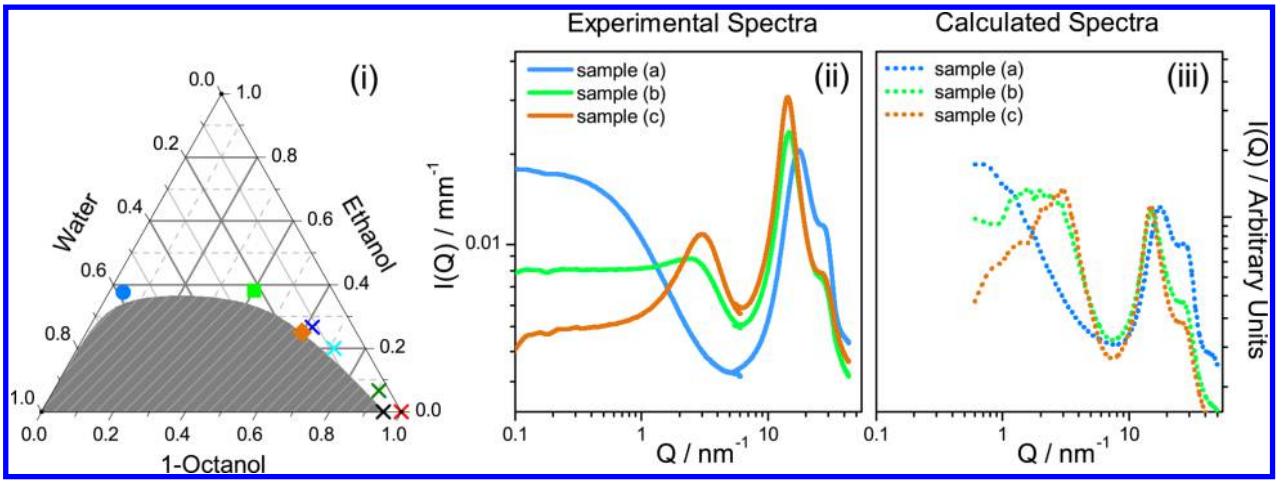

Figure 2. (i) Compositions of the three spectra in wt %. The pre-Ouzo spectrum is depicted as a blue circle, the spectrum in the intermediate region as a green square, and the one corresponding to the region with reverse aggregates as a red diamond. Additionally, the compositions of the five spectra. (ii) Experimental SWAXS spectra of the compositions given in Figure 2 (i) for the three domains. (iii) Simulated SAXS spectra, derived from molecular dynamics at compositions given in Figure 2 (i). Again, the blue spectrum corresponds to the pre-Ouzo regime, the green spectrum to the bicontinuous region, and the red spectrum to the region with reverse aggregates.

correlation between hydroxyl groups, since OH groups possess a higher electronic density than the aliphatic bulk (which is predominantly CH_2).[15] As mentioned before, alcohol moieties tend to group together, forming nodes of a hydrogen-bond network in dry octanol.[21] Comparing wet (black dashed curve) to dry octanol (dashed in red), the peak shows a higher intensity and shifts slightly toward lower Q-values, which can be related to the accumulation of water at the center of the nodes, causing them to swell. Considering that water reorients octanol molecules to form reverse aggregates, the polar cores exhibit a higher electron density than the aliphatic bulk region, which leads to a higher amplitude. Furthermore, the displacement of the peak toward lower Q-values reflects that the distance between the electron-dense clusters is slightly increasing (from 4.1 nm^{-1} to 3.5 nm^{-1}, corresponding to real space distances of 1.5 to 1.8 nm).

Adding ethanol to a partially water containing octanol phase leads always to a displacement of the peak toward lower Q-values, compared to dry octanol. At 20 wt % (cyan curve) and 26 wt % ethanol (blue curve) the position of the peak is at even smaller Q-values than wet octanol (3.3 nm^{-1} and 3.15 nm^{-1} respectively), implying that, by adding ethanol, the average distance between the swollen nodes can be even further increased. It should further be noticed that the intensities in the small-angle regime for wet and dry octanol, as well as for the sample with 6.7 wt % ethanol, are similar and the peak is shifted to very low Q. In contrast, for higher concentrations of hydrotrope, the signal at very low Q-values gradually increases. This is related to an increase of the compressibility of the solution, which is thermodynamically connected to the $S(0)$-value of the structure factor.[34]

Thus, from a qualitative analysis of the SWAXS spectra, it can be concluded that, by adding ethanol, the reverse aggregates remain present after introduction of a hydrotrope to the system.

Comparative Experimental and Theoretical Analysis To Evaluate the Structuration along the Phase Transition beyond the Pre-Ouzo Domain. As illustrated in Figure 2ii, three experimental SWAXS spectra were collected for octan-1-ol/ethanol/water at different compositions, depicted in Figure 2i. As in Figure 1, the curves converge in the WAXS regime, above 7 nm^{-1}. While the aliphatic correlation peak of ethanol and octanol can be found around 14 nm^{-1}, the signature peak of water is localized at 20 nm^{-1} (see Figure S1: spectra of the pure solvents). Therefore, the position of the peak of sample (a) is slightly shifted toward higher Q-values (Q = 17.8 nm^{-1}), due to the higher water content. For sample (c), the opposite is found: The position of the peak remains at Q = 14.7 nm^{-1} as in Figure 1, due to the low amount of water in the solution. With an intermediate intensity, sample (b) shows a signal between the two extremes, where the position of the peak is at Q = 15.1 nm^{-1}. Indeed, Diat et al. demonstrated that the WAXS signal for mixtures of three solvents can be approximately estimated by superposition of the pure solvent spectra.[3]

The spectrum of sample (a) in Figure 2ii shows by far the highest intensity at low Q-values. The composition of the sample was chosen to be in the previously reported pre-Ouzo regime and is not directly situated at the phase border, but several weight percent of ethanol above the binodal.[8] The signal indicates the formation of agglomerates in the nanometer scale. In order to estimate the size of these aggregates, the Ornstein–Zernike equation was applied. We obtain a value $I_{Q=0}$ = 0.019 mm^{-1} for the zero-angle intensity, and a value of ξ = 0.8 nm for the correlation length, which is a measure for the size of the aggregates. This result is in good agreement with reports in previous works[1,4,13] and proves the presence of mesoscopic objects.

A similar slope is found for the spectrum in the intermediate regime (sample (b)) between 3 nm^{-1} and 6 nm^{-1}. However, at lower Q-values, a plateau appears with an intensity that is much lower than for the pre-Ouzo spectrum. Concerning the intermediate spectrum, similar SAXS profiles were reported for bicontinuous microemulsions, where no correlation peak was found at low Q-values. Such systems have been called "flexible bicontinuous microemulsions".[35] Thus, our result supports the hypothesis of such a bicontinuity also in the present case, which has also been inferred from recent conductivity data, which were measured in the same regime of the phase diagram.[22] Finally, the intensity at low Q angles is very low for samples in the region with supposed reverse

DOI: 10.1021/acscentsci.6b00116
ACS Cent. Sci. 2016, 2, 467–475

aggregates, represented by sample (c), with a similar shape of the intensity as demonstrated in the previous paragraph.

Complementary to experimental X-ray scattering, atomistic molecular dynamics simulations have been conducted with systems of the same composition as the experimental ones. The calculated X-ray scattering intensities are illustrated in Figure 2iii. Scattering spectra represent the signal of the totality of aggregates in solution, and, in case of polydispersity, interpretations become scarce.

The theoretical wide-angle regime shows the same tendencies as the experimental results, with the correlation peaks for aliphatic chains and water at the same Q-values. For sample (a), the peak is shifted to $Q = 18$ nm^{-1} as well, due to the higher water content, while it stays around $Q = 14.7$ nm^{-1} for samples (b) and (c). In the small-angle regime, the three spectra show once again profiles very similar to the experimental ones.

Sample (a) shows a typical Ornstein−Zernike behavior, while sample (c) shows a slightly sharper structure peak at $Q = 3$ nm^{-1}. The intermediate spectrum shows the same tendencies at low Q-values, with the indication of a peak at 2.1 nm^{-1} and the formation of a plateau at lower angles. Note that simulation predictions of $I(Q)$ for even smaller angles are not feasible, due to the necessity of bigger simulation boxes.

However, it is quite remarkable that all three scattering length density profiles regarding structuring in the mesoscale domain are overlapping to a large degree. This is shown in detail in the Supporting Information, where a detailed comparison of experimental and calculated intensity spectra can be found (Figures S2-A and -B and Tables S1-A and -B).

In agreement with the experimental data set, the theoretical spectra demonstrate the presence of three different types of mesoscopic structures: direct micelle-like pre-Ouzo aggregates, bicontinuous structures, and swollen reverse water pools, surrounded by 1-octanol and ethanol headgroups.

We now analyze the structural differences between the three regimes on a molecular level. Figure 3 depicts representative

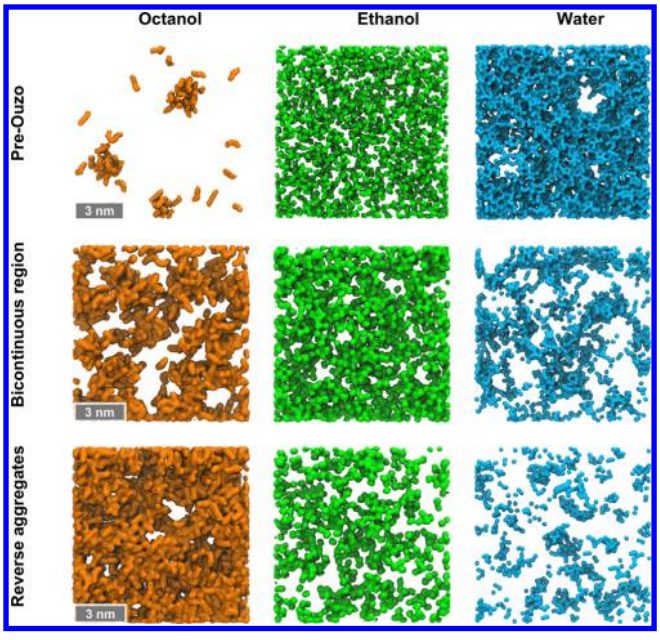

Figure 3. Snapshots of the three regions. Shown are slices of 2 nm thickness for each of the components in a surface representation.

renderings of 2 nm slices through the simulation boxes for octanol, ethanol, and water, respectively. In the pre-Ouzo region, one finds several small clusters of octanol along with a few monomers that show up as holes in the excess water domain. Ethanol is essentially distributed uniformly throughout the system.

Besides forming an interfacial film, it is also present inside the octanol aggregates. In the octanol-rich region of the ternary phase diagram, the situation is inversed: holes in the octanol domain correspond to numerous agglomerates of water molecules. Ethanol is also absent in some areas of the system, because most of it is accumulated at the octanol/water interface. This is supported by the picture given in Figure S3, showing a surface representation of water and all the hydroxyl groups in the segment, which characterizes these water agglomerates as reverse aggregates, swollen by ethanol. Between these two regimes of aggregation we find a bicontinuous region, in analogy to observations in classical water−oil−surfactant systems.[36]

In the bicontinuous region of the phase diagram, water and octanol each form a sponge-like interwined network. Similar to the pre-Ouzo regime, ethanol is distributed evenly in the simulation box. The probability of finding an infinite aggregate of octanol, judged by finding an aggregate that extends continuously through the whole simulation box, is 1, and therefore the system is continuous in octanol. For a characterization of the water domain, we employ commonly used criteria denoting percolation in three dimensions (with a corresponding plot in Figure S4):[37−39] (1) the probability of finding an infinite cluster is above 50%, (2) the cluster size histogram follows a power law with exponent −2.19, and (3) the infinite cluster is a fractal object with dimension $d_f > 2.53$. Our analysis shows a probability of the spanning cluster of 89.5%, a power-law exponent of −2.09 in reasonable agreement with the theoretical value −2.19, and a dimensionality of the infinite cluster of $d_f = 2.78$. The composition is thus well beyond the percolation threshold of water, resulting in continuity both in octanol and in water.

To conclude the first part of the presented work, the combined experimental and theoretical analysis allowed us to confirm that direct micelle-like aggregates are present in the pre-Ouzo regime. Furthermore, the simulations give proof that reverse aggregates are still present on the water-rich side of the phase diagram. The gap between these two regimes is closed by a bicontinuous regime, where phase inversion from a water-continuous to octanol-continuous system occurs. This allows us to define a new mapping of the phases, which is depicted in Figure 4. The structures are the more defined the closer the composition is situated to the phase boundary. With increasing addition of ethanol the aggregation develops more and more into a molecular solution, which is indicated by a color gradient in Figure 4. Note that, in addition to the data shown here, other compositions were investigated with the help of SWAXS experiments along two dilution lines. The results and discussion of these data are given in Figures S5-A and -B.

Miscibility Gap Influenced by the Presence of Sulfuric Acid: Crossing of the Binodals. One quite stunning discovery is the change in the phase transition borders of the pseudoternary system and of the tie lines, when adding sulfuric acid to water. As depicted in Figure 5i (phase diagram in mass fractions), the monophasic region is increasing on the water-rich side of the diagram with increasing acidic concentration, ranging from 0 M to 4 M. On the other hand, the area of the

DOI: 10.1021/acscentsci.6b00116
ACS Cent. Sci. 2016, 2, 467−475

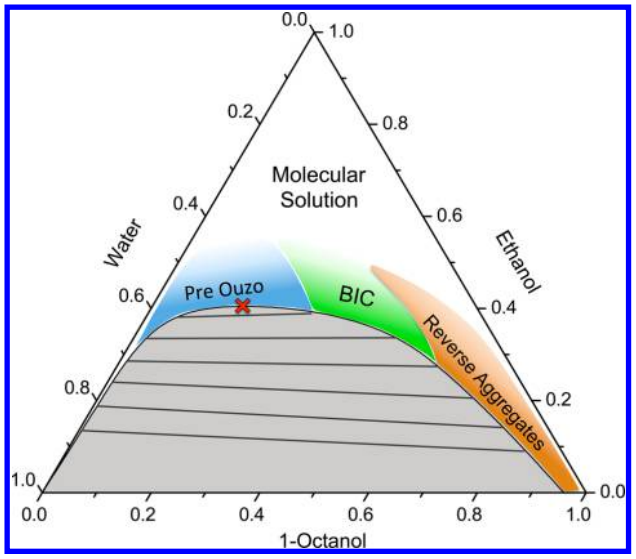

Figure 4. Schematic view of the mesoscopic structuring in the ternary phase diagram 1-octanol/ethanol/water. The region around the phase transition border is dominated by 3 different regimes, which are less pronounced, the more the system is diluted with ethanol. The black lines are the experimentally determined tie lines.

two-phase region increases on the oil-rich side, which can be clearly seen when converting the phase diagram into molar fractions (Figure 5ii). As a result, there is a crossing of the binodals.

Referring to the maximum amount of added ethanol, the maximum of the binodal is reduced from 38 wt % for pure water, down to 26 wt % for the 4 M aqueous sulfuric acid solution. The increase appears to be linear in acid concentration. The decrease of the monophasic region, on the octanol-rich side, is less pronounced. The phase transitions do not coincide at the same composition, but the intercept with respect to the acid-free sample is shifted more and more to the octanol-rich side, the higher the acidic concentration. Considering the different types of molecular structuring introduced in the first part of this work, the sulfuric acid is stabilizing the pre-Ouzo aggregates, while it impedes the formation of reverse aggregates.

The three possible origins of increased repulsions in the presence of sulfuric acid could be as follows:

(a) A "secondary hydration force", which includes the hydration of the electrolyte present, as proposed by Marcelja:[40] the modification of the hydration force by concentrated electrolytes, i.e., when hydration force decay and Debye screening length are both smaller than Bjerrum length, a phenomenon that is ubiquitous, as reviewed recently.[41]

(b) Alternatively, an increased accumulation of ethanol in the interfacial region, which requires a free energy cost to remove.

(c) An accumulation of ethanol, with a decay length of 2−3 nm of the concentration of the hydrotrope on the water-rich side of the interface between the pseudophases. This could be considered conceptually as a "diffuse layer of hydrotropes". Two diffuse layers have a cost in free energy to overlap, as in the general mechanism associated with any order parameter initially proposed by Marcelja[42] and that seems also very ubiquitous.[43] In the present state of knowledge and understanding of UFME stability and of resilience versus added species, these two effects combined on the top of any possible "antagonistic" ion stabilizing effect.

In the phase diagrams studied here, we found that, below 2 M, the effects of adding sulfuric acid are minor. The stabilization and destabilization induced by sulfuric acid is much more pronounced when sulfuric acid is at concentrations 3 M or higher. Any of the three possible physical origins discussed above would explain this behavior. In the present state of knowledge, we do not know which one of the three mechanisms (a), (b), or (c) is dominant.

The progression of the binodal lines is thus the result of the two opposing features, the additional stabilization of pre-Ouzo structures (*salting-in*) in the water-rich region and the *salting-out* of water out of octanol in the octanol-rich region. Note that also the partition of ethanol is significantly shifted toward a higher ethanol concentration in the aqueous phase. This can be seen by the change in the slope of the tie lines, as represented in Figure 6.

To check whether the aggregates are still present after addition of sulfuric acid, SWAXS spectra have been recorded in each of the three regimes. A thorough qualitative analysis is neglected here, since our objective is merely to qualitatively assess whether the structures survive such high concentrations of sulfuric acid or if they experience serious structural rearrangements. The compositions of the spectra are shown in the phase diagram of Figure 6, where the amount of water (in wt %) is replaced by the same amount of aqueous sulfuric acid solution (also in wt %). It should be noted that the significant amount of sulfuric acid slightly changes the density, which would lead to different points in diagrams based on volume or mole fractions. As depicted in Figure 7 the shape of the spectra remains roughly the same and thus confirms that the aggregates are still present at 2 M sulfuric acid. All three

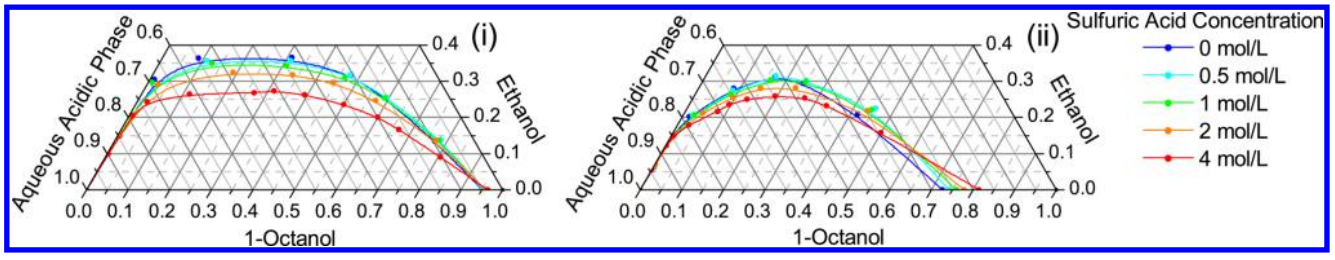

Figure 5. Phase diagram of 1-octanol/ethanol/aqueous sulfuric acid in (i) wt % and (ii) mol %, at different acidic concentrations and at 25 °C; the "aqueous phase" takes into account both water and sulfuric acid, for weight and mole fraction calculations. The blue line is the binodal line for 0 M, the light blue one for 0.5 M, the green one for 1 M, the orange one for 2 M, and the red one for 4 M. See Figure S6 for alternative pseudoternary interpretation.

DOI: 10.1021/acscentsci.6b00116
ACS Cent. Sci. 2016, 2, 467−475

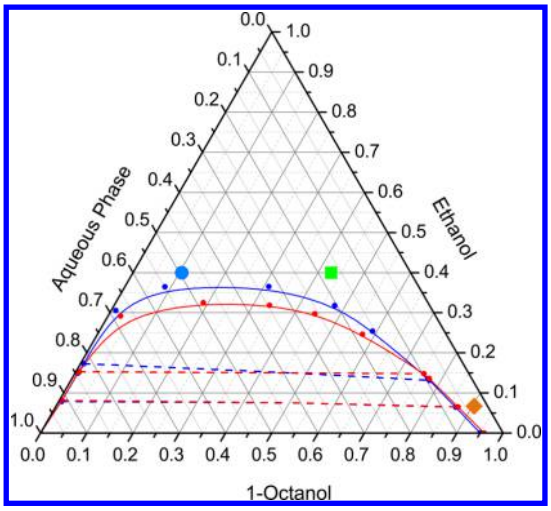

Figure 6. Pseudoternary phase diagram of sulfuric acid/ethanol/1-octanol in wt %. The phase transition for pure water is given in blue, for 2 M sulfuric acid in red. Two tie lines are given for each case (blue tie lines for pure water and red tie lines for 2 M acid, respectively. The composition of the three samples, for which SAXS spectra have been recorded, is also indicated.

spectra have a higher intensity in the low-angle scattering regime, compared to the ternary systems without acid. The introduction of the electron-dense sulfur enhances the scattering contrast, which leads to an increase of intensity.

CONCLUSION AND OUTLOOK

By performing SWAXS experiments on different monophasic water−ethanol−octanol mixtures along the miscibility gap in the phase diagram, we observe fundamental changes in the nanostructuring of the system: the pattern evolves from a typical Ornstein−Zernike behavior in the water-rich pre-Ouzo domain to a bicontinuous region with a characteristic plateau at low Q and finally to the octanol-rich region, for which more or less connected w/o domains predominate in a way similar to reverse connected w/o aggregations. Thus, we can draw an analogy toward the morphology transitions in microemulsions containing surfactants. A yet open question is the phase-transition mechanism, which will be the focus of interest for future works. In the pre-Ouzo region, the single-phase domain is enlarged by the addition of sulfuric acid, due to an additional hydration force repulsion, caused by the presence of the electrolyte.

By contrast, in the octanol-rich domain of the phase diagram, the monophasic region is reduced, because sulfuric acid reduces the amount of water dissolved in octanol in equilibrium with the aqueous solution.

These different structures and their modifications in the presence of a significant amount of electrolytes may have significant consequences on various applications. As already shown, they influence biochemical reactions as well as extraction processes. Probably, even chemical reactions can be optimized by a proper tuning of these highly dynamic nanoconfinements, but this will be the topic of future research.

EXPERIMENTAL SECTION

Materials. Octan-1-ol (purity >99%, for simplicity referred to as "octanol") was purchased from Sigma-Aldrich Chemie GmbH (Steinheim, Germany). Ethanol (purity >99.5%) and sulfuric acid (96 wt %) were provided by Carlo Erba Reagents (Cornaredo, Italy). All samples were prepared with deionized water, with a conductivity of 6.5−12.3 μS·cm^{-1}. The solvents were used without any further purification steps. The term *dry octanol* is attributed to noncontacted octanol, without any drying procedures. The water content from contact with the environment was found to be 452 ppm and determined by coulometric Karl Fischer titration.

Phase Diagrams. All phase diagrams were determined with the cloud point method, by initially mixing ethanol with one of the other two solvents, then adding the third one until the clear solution becomes turbid. The initial diagrams were determined in mass fractions ω_i. To obtain the phase diagram in volume fractions Φ_i the densities of the pure solvents were used, assuming ideal mixing behavior. To obtain the phase diagrams in molar fractions x_i, the molar masses of the pure solvents were used. All diagrams were determined at 25 °C.

SAXS Measurements. Small and wide angle X-ray scattering (SWAXS) data were acquired at the ID02 beamline at the European Synchrotron Radiation Facility (ESRF, Grenoble, France). A wavelength of 12.46 keV (λ = 0.0995 nm) was chosen. Two CCD detectors from Rayonix were used (MX170-HS and LX170-HS respectively for SAXS and WAXS), with a geometry allowing simultaneous acquisition with an overlap in Q, the magnitude of the wavevector,

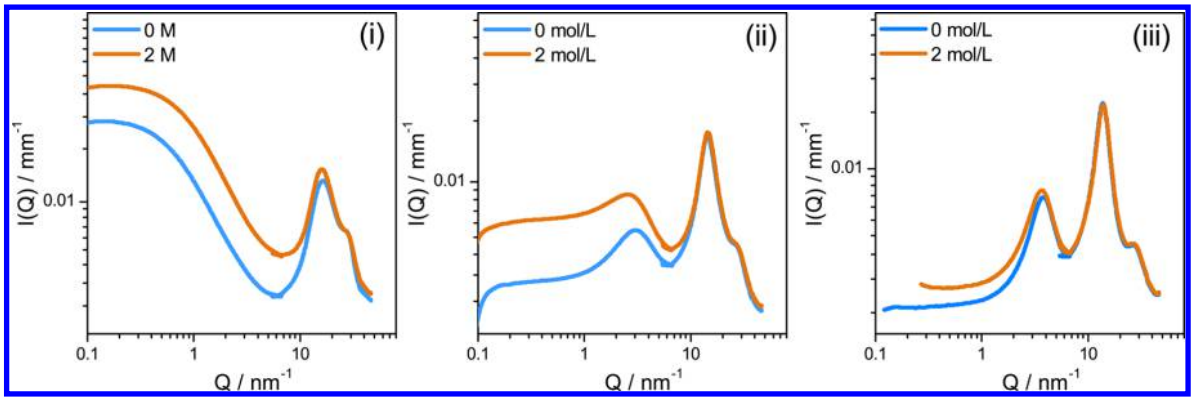

Figure 7. SWAXS spectra in the presence (blue spectra) and absence (orange spectra) of sulfuric acid in the three designated regions: (i) direct pre-Ouzo, (ii) bicontinuous, and (iii) reverse aggregates.

DOI: 10.1021/acscentsci.6b00116
ACS Cent. Sci. 2016, 2, 467−475

$$Q = \frac{4\pi}{\lambda}\cdot\sin\left(\frac{\theta}{2}\right)$$

where θ is the scattering angle as commonly defined. This configuration requires an air gap of ca. 15 cm, causing an increased signal mostly corrected by subsequent background subtraction. The sample-to-detector distances were 1.5 m for the SAXS detector and 0.13 m for the WAXS, as calibrated by the Bragg peaks of *p*-bromobenzoic acid (SAXS and WAXS), silicon (WAXS), and silver behenate (SAXS). Samples were inserted in a thermalized flow-through quartz capillary of inner diameter 1.7 mm. The data were corrected for the dark current, the flat field, and the transmitted beam as measured by a PIN diode on the beam stop; note that effects from the beam polarization and the sample geometry were not taken into account during data reduction. An absolute scale was obtained using the low-Q intensity level of water (at 1.63×10^{-3} mm^{-1} at 25 °C). The scattering from the empty capillary was subtracted. At low Q, a significant part of the scattering comes from surface roughness of the quartz capillary, and is therefore poorly corrected, as the inner interfaces of the capillary have different contrasts depending on the capillary filling. This often results in a small upturn or downturn of the intensity as seen in the various spectra presented hereafter.

SAXS Fit Functions. To determine the correlation length and radii of the pre-Ouzo aggregates, the Ornstein−Zernike (OZ) equation was used as a model, given by[44]

$$I(Q) = \frac{I_0}{1 + \xi^2 Q^2} = \frac{I_0}{1 + \frac{R_G^2 Q^2}{3}}$$

with the correlation length ξ, the radius of gyration R_G, the scattering vector Q, and the intensity I_0 for Q = 0. Full fitting of the spectra using refined expressions is out of the scope of this paper.[45]

Molecular Dynamics. The simulations were performed using the software GROMACS 4.6.[46] The systems are sampled as cubic boxes of variable edge lengths (controlled by temperature and pressure coupling, see below) with periodic boundary conditions applied in all directions.

System Compilation. Simulation boxes of 11 to 12 nm edge lengths were filled with the three components, octanol, ethanol, and water, inserting new molecules at random positions. The system chosen to represent the pre-Ouzo regime contains 224 molecules of octanol, 6366 molecules of ethanol, and 25380 water molecules. The intermediate system consists of 2088 octanol, 5608 ethanol, and 8303 water molecules. The system on the water-poor side of the phase diagram is filled with 3000 octanol, 3600 ethanol, and 5400 water molecules.

First, excessive forces in the systems were eliminated applying a steepest descent algorithm. The resulting configurations were then equilibrated for 100 000 steps at 3 fs/step using the parameters for the production run described in the next paragraph but employing a Berendsen barostat.[47]

Simulation Parameter. We employed the TIP4P/2005[48] model for water and the OPLS all-atom force field[49] for ethanol and octanol. For octanol, special torsional parameters for long hydrocarbons were used.[50] van der Waals interactions were described by a Lennard-Jones potential with a 1 nm cutoff. Electrostatic interactions were calculated according to the smooth particle mesh Ewald (PME) algorithm.[51] The temperature was set to 300 K applying the velocity rescaling algorithm while the pressure was held at 1.0 bar by means of a Parrinello−Rahman barostat.[52] The time constant for both procedures was 1 ps, and a compressibility of 4.5×10^{-5} bar^{-1} was assumed for the barostat. Bond lengths were constrained to their equilibrium positions using the LINCS algorithm, and hydrogen atoms were represented by virtual interaction sites. The leapfrog scheme was employed as an integration method, using a time step of 5 fs.

The water-rich system was sampled for 700 ns while the intermediate and octanol-rich regimes were both simulated for 200 ns.

Analysis. The program nMOLDYN[53] was used to calculate the partial static coherent structure factors from MD trajectories. The partial intensities were derived using the relation $I(Q) \sim S(Q)\cdot f_1(Q) f_2(Q)$, where $f_i(Q)$ are the atomic form factors of the scattering particles. These partial intensities were normalized and summed up to obtain the overall intensity.

A distance criterion is used to identify molecular clusters of water or of octanol. For water, an O−O distance of 0.35 nm was used as a cutoff. In the case of octanol, the carbon and hydroxyl group atoms are considered and the cutoff was set to 0.478 nm, the first distinct minimum in the radial distribution function of this subset in bulk octanol. Other values for these cutoffs lead to slightly different results, but the general observations are qualitatively not influenced.

■ ASSOCIATED CONTENT

Supporting Information

The Supporting Information is available free of charge on the ACS Publications website at DOI: 10.1021/acscentsci.6b00116.

SWAXS and MD details and phase diagrams (PDF)

■ AUTHOR INFORMATION

Corresponding Author

*E-mail: dominik.horinek@chemie.uni-regensburg.de.

Notes

The authors declare no competing financial interest.

■ ACKNOWLEDGMENTS

We acknowledge the European Synchrotron Radiation Facility for provision of synchrotron radiation facilities, and we would like to thank the ID02 team for assistance in using SAXS-WAXS beamline ID02. The research leading to these results has received funding from the European Research Council under the European Union's Seventh Framework Programme (FP/2007-2013)/ERC Grant Agreement No. [320915] "REE-CYCLE": Rare Earth Element reCYCling with Low harmful Emissions. The LABEX "Chemisyst" ANR 2011-01-05 contract is thankfully acknowledged for an invited Professorship supporting one of us (W.K.). The L.I.A. *RECYCLING* French-German CNRS/INC and MPIKG cooperating is thanked for support of French-German exchanges allowing the present work to be performed.

■ REFERENCES

(1) Klossek, M. L.; Touraud, D.; Zemb, T.; Kunz, W. Structure and Solubility in Surfactant-Free Microemulsions. *ChemPhysChem* **2012**, *13*, 4116−4119.

(2) Robertson, A. E.; Phan, D. H.; Macaluso, J. E.; Kuryakov, V. N.; Jouravleva, E. V.; Bertrand, C. E.; Yudin, I. K.; Anisimov, M. A. Mesoscale solubilization and critical phenomena in binary and quasi-

DOI: 10.1021/acscentsci.6b00116
ACS Cent. Sci. 2016, 2, 467−475

binary solutions of hydrotropes. *Fluid Phase Equilib.* **2016**, *407*, 243−254.
(3) Diat, O.; Klossek, M. L.; Touraud, D.; Deme, B.; Grillo, I.; Kunz, W.; Zemb, T. Octanol-rich and water-rich domains in dynamic equilibrium in the pre-ouzo region of ternary systems containing a hydrotrope. *J. Appl. Crystallogr.* **2013**, *46*, 1665−1669.
(4) Schöttl, S.; Marcus, J.; Diat, O.; Touraud, D.; Kunz, W.; Zemb, T.; Horinek, D. Emergence of surfactant-free micelles from ternary solutions. *Chem. Sci.* **2014**, *5*, 2949−2954.
(5) Marcus, J.; Klossek, M. L.; Touraud, D.; Kunz, W. Nano-droplet formation in fragrance tinctures. *Flavour Fragrance J.* **2013**, *28*, 294−299.
(6) Marcus, J.; Müller, M.; Nistler, J.; Touraud, D.; Kunz, W. Nano-droplet formation in water/ethanol or isopropanol/mosquito repellent formulations. *Colloids Surf., A* **2014**, *458*, 3−9.
(7) Klossek, M. L.; Touraud, D.; Kunz, W. Eco-solvents − cluster-formation, surfactantless microemulsions and facilitated hydrotropy. *Phys. Chem. Chem. Phys.* **2013**, *15*, 10971−10977.
(8) Zemb, T.; Klossek, M. L.; Lopian, T.; Marcus, J.; Schöettl, S.; Horinek, D.; Prévost, S. F.; Touraud, D.; Diat, O.; Marčelja, S.; Kunz, W. How to explain microemulsions formed by solvent mixtures without conventional surfactants. *Proc. Natl. Acad. Sci. U. S. A.* **2016**, *113*, 4260−4265.
(9) Xenakis, A.; Zoumpanioti, M.; Stamatis, H. Enzymatic reactions in structured surfactant-free microemulsions. *Curr. Opin. Colloid Interface Sci.* **2016**, *22*, 41−45.
(10) Smith, G. D.; Donelan, C. E.; Barden, R. E. Oil-continuous microemulsions composed of hexane, water, and 2-propanol. *J. Colloid Interface Sci.* **1977**, *60*, 488−496.
(11) Schöttl, S.; Horinek, D. Aggregation in detergent-free ternary mixtures with microemulsion-like properties. *Curr. Opin. Colloid Interface Sci.* **2016**, *22*, 8−13.
(12) Leontidis, E.; Christoforou, M.; Georgiou, C.; Delclos, T. The ion-lipid battle for hydration water and interfacial sites at soft-matter interfaces. *Curr. Opin. Colloid Interface Sci.* **2014**, *19*, 2−8.
(13) Marcus, J.; Touraud, D.; Prévost, S.; Diat, O.; Zemb, T.; Kunz, W. Influence of additives on the structure of surfactant-free microemulsions. *Phys. Chem. Chem. Phys.* **2015**, *17*, 32528−32538.
(14) Sangster, J. *Octanol-Water Partitioning Coefficients: Fundamentals and Physical Chemistry*; John Wiley & Sons: Chichester, U.K., 1997.
(15) Franks, N. P.; Abraham, M. H.; Lieb, W. R. Molecular Organization of Liquid n-Octanol: An X-ray Diffraction Analysis. *J. Pharm. Sci.* **1993**, *82*, 466−470.
(16) Marcus, Y. Structural aspects of water in 1-octanol. *J. Solution Chem.* **1990**, *19*, 507−517.
(17) Lawrence, A. S. C.; McDonald, M. P.; Stevens, J. V. Molecular association in liquid alcohol-water systems. *Trans. Faraday Soc.* **1969**, *65*, 3231.
(18) Grunwald, E.; Pan, K.-C.; Effio, A. Hydrogen bonding in polar liquid solutions. 4. Effect of hydrogen-bonding solutes on dielectric constant and solvent structure in 1-octanol. *J. Phys. Chem.* **1976**, *80*, 2937−2940.
(19) Best, S. A.; Merz, K. M., Jr.; Reynolds, C. H. Free Energy Perturbation Study of Octanol/Water Partition Coefficients: Comparison with Continuum GB/SA Calculations. *J. Phys. Chem. B* **1999**, *103*, 714−726.
(20) MacCallum, J. L.; Tieleman, D. P. Structures of Neat and Hydrated 1-Octanol from Computer Simulations. *J. Am. Chem. Soc.* **2002**, *124*, 15085−15093.
(21) Chen, B.; Siepmann, J. I. Microscopic Structure and Solvation in Dry and Wet Octanol. *J. Phys. Chem. B* **2006**, *110*, 3555−3563.
(22) Bošković, P.; Sokol, V.; Zemb, T.; Touraud, D.; Kunz, W. Weak Micelle-Like Aggregation in Ternary Liquid Mixtures as Revealed by Conductivity, Surface Tension, and Light Scattering. *J. Phys. Chem. B* **2015**, *119*, 9933−9939.
(23) Tanford, C. *The Hydrophobic Effect: Formation of Micelles and Biological Membranes*; John Wiley & Sons Inc.: Chichester, U.K., 1980.
(24) Israelachvili, J. N.; Mitchell, D. J.; Ninham, B. W. Theory of self-assembly of hydrocarbon amphiphiles into micelles and bilayers. *J. Chem. Soc., Faraday Trans. 2* **1976**, *72*, 1525−1568.
(25) Schöttl, S.; Touraud, D.; Kunz, W.; Zemb, T.; Horinek, D. Consistent definitions of "the interface" in surfactant-free micellar aggregates. *Colloids Surf., A* **2015**, *480*, 222−227.
(26) Burant, A.; Lowry, G. V.; Karamalidis, A. L. Measurement of Setschenow constants for six hydrophobic compounds in simulated brines and use in predictive modeling for oil and gas systems. *Chemosphere* **2016**, *144*, 2247−2256.
(27) Arce, A.; Blanco, A.; Soto, A.; Vidal, I. Densities, refractive indices, and excess molar volumes of the ternary systems water + methanol + 1-octanol and water + ethanol + 1-octanol and their binary mixtures at 298.15 K. *J. Chem. Eng. Data* **1993**, *38*, 336−340.
(28) Arce, A.; Blanco, A.; Souza, P.; Vidal, I. Liquid-Liquid Equilibria of Water + Methanol + 1-Octanol and Water + Ethanol + 1-Octanol at Various Temperatures. *J. Chem. Eng. Data* **1994**, *39*, 378−380.
(29) Guilbaud, P.; Zemb, T. Solute-Induced Microstructural Transition from Weak Aggregates towards a Curved Film of Surface-Active Extractants. *ChemPhysChem* **2012**, *13*, 687−691.
(30) Donaldson, S. H.; Røyne, A.; Kristiansen, K.; Rapp, M. V.; Das, S.; Gebbie, M. A.; Lee, D. W.; Stock, P.; Valtiner, M.; Israelachvili, J. Developing a General Interaction Potential for Hydrophobic and Hydrophilic Interactions. *Langmuir* **2015**, *31*, 2051−2064.
(31) Qiao, B.; Ferru, G.; Olvera de la Cruz, M.; Ellis, R. J. Molecular Origins of Mesoscale Ordering in a Metalloamphiphile Phase. *ACS Cent. Sci.* **2015**, *1*, 493−503.
(32) French, R. H.; Parsegian, V. A.; Podgornik, R.; Rajter, R. F.; Jagota, A.; Luo, J.; Asthagiri, D.; Chaudhury, M. K.; Chiang, Y.; Granick, S.; Kalinin, S.; Kardar, M.; Langreth, D. C.; Lewis, J.; Lustig, S.; Wesolowski, D.; Wettlaufer, J. S.; Ching, W.-Y.; Finnis, M.; Houlihan, F.; von Lilienfeld, O. A.; van Oss, C. J.; Zemb, T. Long range interactions in nanoscale science. *Rev. Mod. Phys.* **2010**, *82*, 1887−1944.
(33) Ellis, R. J.; Meridiano, Y.; Muller, J.; Berthon, L.; Guilbaud, P.; Zorz, N.; Antonio, M. R.; Demars, T.; Zemb, T. Complexation-Induced Supramolecular Assembly Drives Metal-Ion Extraction. *Chem. - Eur. J.* **2014**, *20*, 12685.
(34) Clark, G. N. I.; Hura, G. L.; Teixeira, J.; Soper, A. K.; Head-Gordon, T. Small-angle scattering and the structure of ambient liquid water. *Proc. Natl. Acad. Sci. U. S. A.* **2010**, *107*, 14003−14007.
(35) Duvail, M.; Dufrêche, J.-F.; Arleth, L.; Zemb, T. Mesoscopic modelling of frustration in microemulsions. *Phys. Chem. Chem. Phys.* **2013**, *15*, 7133.
(36) Borkovec, M.; Eicke, H.-F.; Hammerich, H.; Das Gupta, B. Two percolation processes in microemulsions. *J. Phys. Chem.* **1988**, *92*, 206−211.
(37) Oleinikova, A.; Brovchenko, I.; Geiger, A.; Guillot, B. Percolation of water in aqueous solution and liquid-liquid immiscibility. *J. Chem. Phys.* **2002**, *117*, 3296−3304.
(38) De Candia, A.; Del Gado, E.; Fierro, A.; Sator, N.; Coniglio, A. Colloidal gelation, percolation and structural arrest. *Physica A* **2005**, *358*, 239−248.
(39) Jan, N. Large lattice random site percolation. *Phys. A* **1999**, *266*, 72−75.
(40) Marcelja, S. Hydration in electrical double layers. *Nature* **1997**, *385*, 689−690.
(41) Marčelja, S. Hydration forces near charged interfaces in terms of effective ion potentials. *Curr. Opin. Colloid Interface Sci.* **2011**, *16*, 579−583.
(42) Marcelja, S.; Radić, N. Repulsion of interfaces due to boundary water. *Chem. Phys. Lett.* **1976**, *42*, 129−130.
(43) Parsegian, V. A.; Zemb, T. Hydration forces: Observations, explanations, expectations, questions. *Curr. Opin. Colloid Interface Sci.* **2011**, *16*, 618−624.
(44) Gawrys, K. L.; Blankenship, A. G.; Kilpatrick, R. K. Solvent Entrainment in and Flocculation of Asphaltenic Aggregates Probed by Small-Angle Neutron Scattering. *Langmuir* **2006**, *22*, 4487−4497.

DOI: 10.1021/acscentsci.6b00116
ACS Cent. Sci. 2016, 2, 467−475

(45) Onuki, A.; Kitamura, H. Solvation effects in near-critical binary mixtures. *J. Chem. Phys.* **2004**, *121* (7), 3143−3151.
(46) Hess, B.; Kutzner, C.; van der Spoel, D.; Lindahl, E. GROMACS 4: Algorithms for Highly Efficient, Load-Balanced, and Scalable Molecular Simulation. *J. Chem. Theory Comput.* **2008**, *4*, 435−447.
(47) Berendsen, H. J. C.; Postma, J. P. M.; DiNola, A.; Haak, J. R. Molecular dynamics with coupling to an external bath. *J. Chem. Phys.* **1984**, *81*, 3684−3690.
(48) Abascal, J. L. F.; Vega, C. A general purpose model for the condensed phases of water: TIP4P/2005. *J. Chem. Phys.* **2005**, *123*, 234505.
(49) Jorgensen, W. L.; Maxwell, D. S.; Tirado-Rives, J. Development and Testing of the OPLS All-Atom Force Field on Conformational Energetics and Properties of Organic Liquids. *J. Am. Chem. Soc.* **1996**, *118*, 11225−11236.
(50) Siu, S. W. I.; Pluhackova, K.; Böckmann, R. A. Optimization of the OPLS-AA Force Field for Long Hydrocarbons. *J. Chem. Theory Comput.* **2012**, *8*, 1459−1470.
(51) Essmann, U.; Perera, L.; Berkowitz, M. L.; Darden, T.; Lee, H.; Pedersen, L. G. A smooth particle mesh ewald potential. *J. Chem. Phys.* **1995**, *103*, 8577−8592.
(52) Parrinello, M.; Rahman, A. Polymorphic transitions in single crystals: A new molecular dynamics method. *J. Appl. Phys.* **1981**, *52*, 7182−7190.
(53) Hinsen, K.; Pellegrini, E.; Stachura, S.; Kneller, G. R. nMoldyn 3: Using task farming for a parallel spectroscopy-oriented analysis of molecular dynamics simulations. *J. Comput. Chem.* **2012**, *33*, 2043−2048.

NOTE ADDED AFTER ASAP PUBLICATION

Due to a production error, this article published July 11, 2016 with an incorrect version of Figure 2. The correct version published July 27, 2016.

DOI: 10.1021/acscentsci.6b00116
ACS Cent. Sci. 2016, 2, 467−475